

Supporting Information for

## **ATRP in Water: Kinetic Analysis of Active and Super-Active Catalysts for Enhanced Polymerization Control**

Marco Fantin,<sup>§,‡</sup> Abdirisak A. Isse,<sup>\*,§</sup> Krzysztof Matyjaszewski,<sup>‡</sup> and Armando Gennaro<sup>§</sup>

<sup>§</sup>Department of Chemical Sciences, University of Padova, via Marzolo 1, 35131, Padova, Italy

<sup>‡</sup>Department of Chemistry, Carnegie Mellon University, Pittsburgh, PA 15213, United States

### **Contents**

S1. Experimental Section .....	2
S2. Determination of $k_{\text{act}}$ by monitoring $[\text{Cu}^{\text{I}}\text{L}]^+$ decay at RDE .....	3
S3. CV of $[\text{Cu}^{\text{II}}\text{TPMA}]^{2+}$ in the Presence of OEOBP at Different Scan Rates .....	6
S4. Determination of Parameters Required for the Simulation of CV .....	6
S5. Construction of the Theoretical Curves for Homogenous Redox Catalysis and Comparison with Experimental $I_p/I_p^0$ data .....	9
S6. Comparison between Experimental and Simulated CVs in the Presence of $[\text{Cu}^{\text{II}}\text{TPMA}]^{2+}$ and OEOBP.....	11
S7. Comparison of the CV Response in the Absence and in the Presence of Monomer .....	12
S7. Estimation of $K_{\text{ATRP}}$ for the $[\text{Cu}^{\text{I}}\text{L}]^+/\text{OEOBP}$ Systems .....	12
References .....	13

## S1. Experimental Section

**Chemicals.** All aqueous solutions were prepared in double distilled water. Copper(II) trifluoromethanesulfonate ( $\text{Cu}(\text{OTf})_2$ , Alpha Aesar, 98%) and tetrakis(acetonitrile)copper(I) tetrafluoroborate ( $\text{Cu}^{\text{I}}(\text{CH}_3\text{CN})_4\text{BF}_4$ , Sigma-Aldrich, 97%) were used without further purification. Stock solutions of  $\text{Cu}^{\text{I}}$  were standardized by spectrophotometric analysis using 2,9-dimethyl-1,10-phenantroline as a specific ligand, as described in the literature.<sup>1</sup> Amine ligands, tris(2-pyridylmethyl)amine (TPMA, ATRP Solutions, 98%), tris[2-(dimethylamino)ethyl]amine ( $\text{Me}_6\text{TREN}$ , Sigma-Aldrich, 98%) and *N,N,N',N'',N''*-pentamethyldiethylenetriamine (PMDETA, Sigma-Aldrich, 98%) were used as received. Oligo(ethylene oxide) methyl ether acrylate (OEOA, Sigma-Aldrich, average  $M_w$  480) was passed through a column filled with basic alumina to remove polymerization inhibitors. *N*-isopropylacrylamide (NiPAM, Sigma-Aldrich, 97%) was recrystallized from *n*-hexane. 2-hydroxyethyl 2-bromoisobutyrate (HEBiB, Sigma-Aldrich, 95%) was used as received. *N*-isopropyl 2-bromopropionamide (NiPBPA) and oligo(ethylene oxide) 2-bromopropionate (OEOBP) were synthesized according to literature procedures.<sup>2,3</sup>

**Cyclic Voltammetry (CV).** CVs were performed by an Autolab PGSTAT30 potentiostat (Eco-Chimie, Utrecht, The Netherlands) interfaced to a PC running an Autolab GPES 4.9 software. A three-electrode cell with a glassy carbon working electrode (3 mm diameter disc, Metrohm) and a Pt counter electrode was used. The reference electrode was a saturated calomel reference electrode (SCE, Schott Gerade). Potential step chronoamperometry experiments were performed using a rotating disc electrode, RDE, with a glassy carbon tip of 3 mm diameter (Autolab, Eco-Chimie). Prior to each experiment, the working electrode surface was cleaned by polishing with 0.25- $\mu\text{m}$  diamond paste, followed by ultrasonic rinsing in ethanol for 5 min.

Digital simulation of voltammetric responses was performed with DigiSim 3.03 (Bioanalytical Systems, Inc.).

## S2. Determination of $k_{\text{act}}$ by monitoring $[\text{Cu}^{\text{I}}\text{L}]^+$ decay at RDE

### *Electrochemical Behavior of $[\text{Cu}^{\text{I}}\text{L}]^+$ at a RDE*

$[\text{Cu}^{\text{I}}\text{L}]^+$  exhibits a well-defined anodic wave at the RDE (linear sweep voltammetry in Figure S1).

The limiting current,  $I_L$ , was used to monitor  $C_{[\text{Cu}^{\text{I}}\text{L}]^+}$  during the activation reaction, according to Levich equation:<sup>4</sup>

$$I_L = 0.62nFAD^{2/3}\omega^{1/2}\nu^{-1/6}C_{[\text{Cu}^{\text{I}}\text{L}]^+} \quad (\text{S1})$$

where  $n$  is the number of exchanged electrons,  $F$  is the Faraday constant,  $D$  is the diffusion coefficient of  $[\text{Cu}^{\text{I}}\text{L}]^+$ ,  $A$  is the area of the electrode,  $\omega$  is the RDE rotation speed and  $\nu$  is the kinematic viscosity.

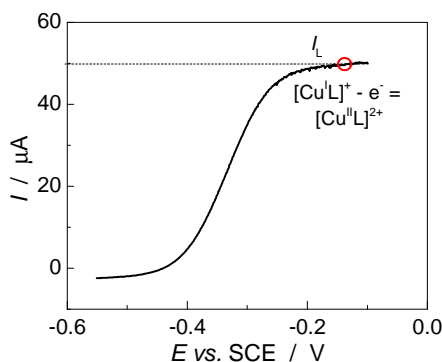


**Figure S1.** Linear sweep voltammetry of  $2 \times 10^{-3}$  M  $[\text{Cu}^{\text{I}}\text{TPMA}]^+$  in  $\text{H}_2\text{O} + 0.1$  M  $\text{Et}_4\text{NBF}_4$  at RDE ( $\omega = 2500$  rpm). The red circle indicates the typical  $E_{\text{app}}$  used to monitor  $\text{Cu}^{\text{I}}$  concentration.

### *Derivation of Kinetic Laws to Determine $k_{\text{act}}$*

Slow reactions were studied under pseudo-first-order conditions with  $C_{\text{RX}}^0 \geq 20C_{[\text{Cu}^{\text{I}}\text{L}]^+}^0$  :

$$\ln C_{[\text{Cu}^{\text{I}}\text{L}]^+} = \ln C_{[\text{Cu}^{\text{I}}\text{L}]^+}^0 - k't \quad (\text{S2})$$

where  $k' = k_{\text{act}}C_{\text{RX}}^0$ .

The concentration of  $[\text{Cu}^{\text{I}}\text{L}]^+$  at any moment during the reaction with RX was calculated from eq S1 as follows:

$$\frac{I_{\text{L}}}{I_{\text{L}}^0} = \frac{0.62nFAD^{2/3}\omega^{1/2}\nu^{-1/6}C_{[\text{Cu}^{\text{I}}\text{L}]^+}}{0.62nFAD^{2/3}\omega^{1/2}\nu^{-1/6}C_{[\text{Cu}^{\text{I}}\text{L}]^+}^0} = \frac{C_{[\text{Cu}^{\text{I}}\text{L}]^+}}{C_{[\text{Cu}^{\text{I}}\text{L}]^+}^0} \quad (\text{S3})$$

where  $I_{\text{L}}^0$  is the limiting current measured for  $[\text{Cu}^{\text{I}}\text{L}]^+$  at  $t = 0$ .

Combining equations S1 and S3 gives

$$\ln(I_{\text{L}}/I_{\text{L}}^0) = -k't \quad (\text{S4})$$

Faster reactions were analyzed under second-order conditions with identical initial concentrations of alkyl halide and  $[\text{Cu}^{\text{I}}\text{L}]^+$ :

$$-\frac{dC_{[\text{Cu}^{\text{I}}\text{L}]^+}}{dt} = k_{\text{act}}C_{[\text{Cu}^{\text{I}}\text{L}]^+}C_{\text{RX}} = k_{\text{act}}C_{[\text{Cu}^{\text{I}}\text{L}]^+}^2 \quad (\text{S5})$$

which upon integration gives:

$$\frac{1}{C_{[\text{Cu}^{\text{I}}\text{L}]^+}} - \frac{1}{C_{[\text{Cu}^{\text{I}}\text{L}]^+}^0} = k_{\text{act}}t \quad (\text{S6})$$

Combining S3 and S6 gives

$$\frac{1}{C_{[\text{Cu}^{\text{I}}\text{L}]^+}} - \frac{1}{C_{[\text{Cu}^{\text{I}}\text{L}]^+}^0} = \frac{I_{\text{L}}^0}{I_{\text{L}}C_{[\text{Cu}^{\text{I}}\text{L}]^+}^0} - \frac{1}{C_{[\text{Cu}^{\text{I}}\text{L}]^+}^0} = k_{\text{act}}t \quad (\text{S7})$$

### ***Experimental Procedure to Determine $k_{\text{act}}$***

Experimentally, a solution of initiator is prepared in an electrochemical cell filled with all electrodes, background electrolyte and a radical scavenger, *e.g.*, TEMPO. Then a constant potential in the plateau region of the oxidation wave of  $\text{Cu}^{\text{I}}$  is applied (see Figure S1) with recording of  $I_{\text{L}}$  and the catalyst is injected. Efficient mixing is ensured by fast magnetic stirring

and by the fast RDE rotating speed (up to 10000 rpm). The output of the experiment is a decay curve for the oxidation current of  $\text{Cu}^{\text{I}}$ , which is consumed during the reaction with RX (Figure S2a, c). Since  $I_L$  is proportional to  $C_{[\text{Cu}^{\text{I}}\text{L}]^+}$ , the curve represents the rate of disappearance of  $[\text{Cu}^{\text{I}}\text{L}]^+$ . Elaboration of the data according to eq S2 or eq S6, depending on the experimental conditions, provides the rate constant,  $k_{\text{act}}$ . Examples of linear plots based on eqs S2 and S6 are reported in Figure S2b, d.

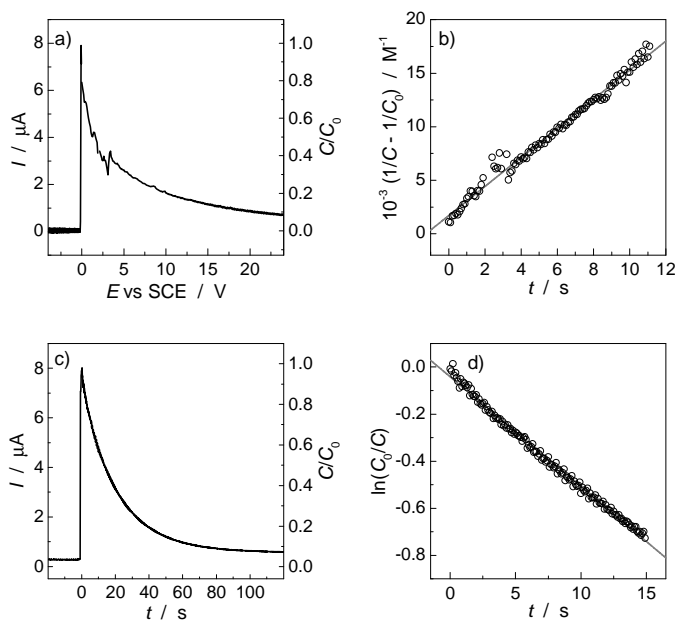


**Figure S2.** Determination of  $k_{\text{act}}$  for the reaction between  $2.5 \times 10^{-4}$  M  $[\text{Cu}^{\text{I}}\text{TPMA}]^+$  and (a, b)  $2.5 \times 10^{-4}$  M OEOBP or (c, d)  $5 \times 10^{-3}$  M NiPBPA in the presence of  $5 \times 10^{-3}$  M TEMPO at 25 °C. (a, c) Variation of  $I_L$  with time recorded at  $E_{\text{app}} = -0.15$  V vs. SCE on RDE ( $\omega = 5000$  rpm). Kinetic analysis according to (b) a second-order (eq S6) or (d) pseudo-first-order rate law (eq S2).

This technique is applicable in both water and organic solvents as long as  $E_{\text{app}}$  is significantly more positive than  $E_{1/2}$  of all the relevant copper complexes present in solution (*i.e.*  $E_{\text{app}}$  is in the plateau region of  $\text{Cu}^{\text{I}}$  oxidation, *e.g.* in Figure S1). First-order conditions are suitable for slow reactions ( $k_{\text{act}} < 10 \text{ M}^{-1} \text{ s}^{-1}$ ), whereas second order conditions ( $C_{[\text{Cu}^{\text{I}}\text{L}]^+}^0 = C_{\text{RX}}^0$ ) are suitable for faster reactions ( $k_{\text{act}} > 1 \text{ M}^{-1} \text{ s}^{-1}$ ).

### S3. CV of $[\text{Cu}^{\text{II}}\text{TPMA}]^{2+}$ in the Presence of OEOBP at Different Scan Rates

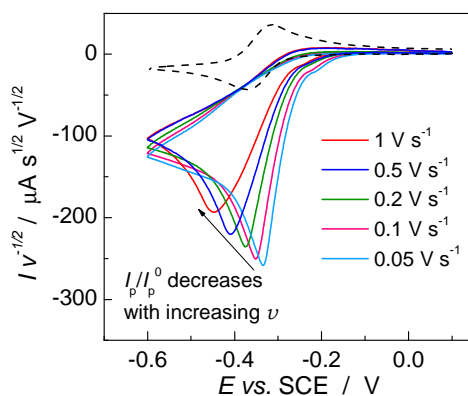


**Figure S3.** Background subtracted CVs of  $10^{-3} \text{ M } [\text{Cu}^{\text{II}}\text{TPMA}]^{2+}$  in  $\text{H}_2\text{O} + 0.1 \text{ M Et}_4\text{NBF}_4$ , recorded at a glassy carbon electrode in the absence (dotted line) and presence (solid lines) of  $5 \times 10^{-3} \text{ M OEOBP}$  at different scan rates ( $I$  was normalized by  $\nu^{1/2}$ ).

### S4. Determination of Parameters Required for the Simulation of CV

The reactions occurring during CV of  $[\text{Cu}^{\text{II}}\text{L}]^+$  in the presence of RX and TEMPO ( $\text{T}^\bullet$ ) are here reported (numeration is the same as in the main text). Thermodynamic and kinetic parameters of interest are reported in the same line.





For all radicals, coupling reactions (eqs 7 and 8) were considered to be very fast with rate constants  $k_{10} = 10^9 \text{ M}^{-1}\text{s}^{-1}$  and  $k_{11} = 10^8 \text{ M}^{-1} \text{ s}^{-1}$ .<sup>5-7</sup>

**Table S1. Thermodynamic Data Used for the Simulation of CV<sup>a</sup>**

Species	$K_{\text{ATRP}}^{\text{b}}$	$K_{\text{Br}^{\text{II}}} (\text{M}^{-1})$	$K_{\text{Br}^{\text{I}}} (\text{M}^{-1})$
$[\text{Cu}^{\text{II}}\text{TPMA}]^{2+}$	0.8	8.05	155
$[\text{Cu}^{\text{II}}\text{Me}_6\text{TREN}]^{2+}$	$8.0 \times 10^{-1}$	4.26	4.26
$[\text{Cu}^{\text{II}}\text{PMDETA}]^{2+}$	$4.6 \times 10^{-2}$	0.84	0.84

<sup>a</sup>From reference <sup>8</sup>. <sup>b</sup>Determined for the reaction of  $[\text{Cu}^{\text{I}}\text{L}]^+$  with HEBiB in water.

The equilibrium constants of  $\text{Br}^-$  association with  $[\text{Cu}^{\text{II}}\text{L}]^{2+}$  and  $[\text{Cu}^{\text{I}}\text{L}]^+$  in water have recently been reported.<sup>8</sup> We used these values for both pure water and aqueous solutions containing 18% monomer (w/w) (Table S1). Additionally, we assumed that the association/dissociation equilibria are fast so that they constitute conditions of pre-equilibrium for the activation step. Therefore, we used a rate constant,  $k_{\text{Br}}$ , of  $10^4 \text{ M}^{-1}\text{s}^{-1}$  for the reaction of  $\text{Br}^-$  with both  $[\text{Cu}^{\text{II}}\text{L}]^{2+}$  and  $[\text{Cu}^{\text{I}}\text{L}]^+$ . Higher values of  $k_{\text{Br}}$  did not affect the degree of catalysis in the simulated CVs.  $K_{\text{ATRP}}$  for the reaction between  $\text{Cu}^{\text{I}}$  complexes and HEBiB in water is in the range 0.05 – 0.80.<sup>8</sup>  $K_{\text{ATRP}}$  values in water/monomer mixtures are not known, but are expected to be smaller than in pure water. The role of  $K_{\text{ATRP}}$  on the simulation was investigated and it was found that simulated CV responses are unaffected provided that  $K_{\text{ATRP}} > 10^{-4}$ .<sup>9</sup> Since this limit is much smaller than the typical  $K_{\text{ATRP}}$  values in aqueous media,<sup>8</sup> the values reported for pure water were used in all aqueous solutions.

$E^{\ominus}$  and  $k^{\ominus}$  of the complexes  $[\text{Cu}^{\text{II}}\text{L}]^{2+}$  as well as the diffusion coefficients of all species were determined by cyclic voltammetry.  $E^{\ominus}$  was measured as the half-sum of the cathodic and anodic peak potentials. The standard reduction potentials of the ternary complexes  $[\text{Br-Cu}^{\text{II}}\text{L}]^+$  could not be measured, but since  $E^{\ominus}_{[\text{X-Cu}^{\text{II}}\text{L}]^+ / [\text{X-Cu}^{\text{I}}\text{L}]} \geq E^{\ominus}_{[\text{Cu}^{\text{II}}\text{L}]^{2+} / [\text{Cu}^{\text{I}}\text{L}]^+}$ , the same values were used for  $[\text{Cu}^{\text{II}}\text{L}]^{2+}$

and  $[\text{Br-Cu}^{\text{II}}\text{L}]^+$ . Diffusion coefficients of the complexes were obtained from the cathodic peak current,  $I_{\text{pc}}$ , according to the following equation valid for a reversible electrode process:<sup>4</sup>

$$I_{\text{pc}} = (2.69 \times 10^5) n^{3/2} A D^{1/2} C \nu^{1/2} \quad (\text{S8})$$

where  $n$  is the number of exchanged electrons,  $A$  is the area of the electrode and  $C$  is the bulk concentration of the  $\text{Cu}^{\text{II}}$  complex. The initiators HEBiB, OEOBP and NiPBPA give a single irreversible reduction peak in cyclic voltammetry (Figure S4) corresponding to a  $2e^-$  reduction of the carbon-bromine bond to RH and  $\text{Br}^-$ . The peak current can be used also in this case to calculate  $D$  according to the following equation:<sup>4</sup>

$$I_{\text{pc}} = (2.99 \times 10^5) \alpha^{1/2} n A D^{1/2} C \nu^{1/2} \quad (\text{S9})$$

where  $C$  is the bulk concentration of RX and  $\alpha$  is the transfer coefficient, which also was determined from the peak characteristics according to known procedures.<sup>10</sup> The equation  $(\partial E_p)/\partial \log \nu = -1.15 RT/\alpha F$  was used, which relates the shift in the reduction peak potential,  $E_p$ , with  $\log \nu$ , to the transfer coefficient,  $\alpha$ . Table S2 summarizes all thermodynamic and kinetic data determined from cyclic voltammetry for Cu complexes and initiators.

**Table S2. Data from Cyclic Voltammetry of  $[\text{Cu}^{\text{II}}\text{L}]^{2+}$  and RX in  $\text{H}_2\text{O}$  and in  $\text{H}_2\text{O} + 18 \text{ wt}\%$  Monomer (OEOA or NiPAM)<sup>a</sup>**

Species	Water			Water/OEOA			Water/NiPAM		
	$E^{\text{e}b}$ (V)	$10^6 D$ ( $\text{cm}^2/\text{s}$ )	$10^3 k^0$ ( $\text{cm}/\text{s}$ )	$E^{\text{e}b}$ (V)	$10^6 D$ ( $\text{cm}^2/\text{s}$ )	$10^3 k^0$ ( $\text{cm}/\text{s}$ )	$E^{\text{e}b}$ (V)	$10^6 D$ ( $\text{cm}^2/\text{s}$ )	$10^3 k^0$ ( $\text{cm}/\text{s}$ )
$[\text{Cu}^{\text{II}}\text{TPMA}]^{2+}$	-0.35	4.6	18	-0.18	0.98	3.1	-0.17	1.1	2.0
$[\text{Cu}^{\text{II}}\text{Me}_6\text{TREN}]^{2+}$	-0.40	2.0	10	-0.34	0.58	1.5	-0.33	0.91	1.0
$[\text{Cu}^{\text{II}}\text{PMDETA}]^{2+}$	-0.37	5.0	5	-0.34			-0.33		
HEBiB	-0.73 <sup>c</sup>	6.0		-1.23	2.0				
OEOBP	-0.81 <sup>c</sup>	3.1		-1.11	0.58				
NiPBPA	-1.34 <sup>c</sup>	8.3					-1.57	3.2	

<sup>a</sup>Data obtained at 25 °C, using 0.1 M  $\text{Et}_4\text{NBF}_4$  as supporting electrolyte. <sup>b</sup>Versus saturated calomel electrode (SCE). <sup>c</sup>Cathodic peak potential at  $\nu = 0.2 \text{ Vs}^{-1}$ .

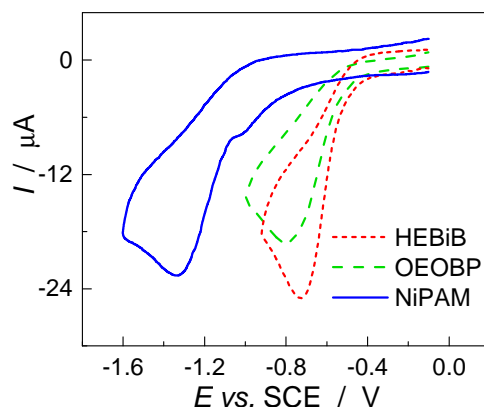


**Figure S4.** CVs of  $10^{-3}$  M RX in  $\text{H}_2\text{O} + 0.1$  M  $\text{Et}_4\text{NBF}_4$ , recorded at a glassy carbon electrode at  $\nu = 0.2$  V  $\text{s}^{-1}$ .

## S5. Construction of the Theoretical Curves for Homogenous Redox Catalysis and Comparison with Experimental $I_p/I_p^0$ data

The degree of catalysis or current enhancement,  $I_p/I_p^0$ , depends on the following kinetic parameter:<sup>11</sup>

$$\lambda = \frac{RTk_{\text{act}}C_{[\text{Cu}^{\text{II}}\text{L}]^{2+}}}{F\nu}$$

Theoretical working curves relating  $I_p/I_p^0$  to  $\lambda$  can be constructed by digital simulation of the voltammetric response of the catalytic system (eqs 2-8). Voltammetric simulations were carried out for a large number of  $\lambda$  values and the results were plotted as  $I_p/I_p^0$  versus  $\log \lambda$  (Figure S5a). To make easy the comparison between experimental and simulated data, the latter were first fit to appropriate functions that perfectly interpolate all data (Figure S5b). Two equations (eqs S10 and S11) were used, depending on whether the theoretical curve presented a maximum or a plateau. Examples of the fittings are reported in Figure S5.

$$y = a + b \left[ \frac{c}{1 + \exp\left(\frac{x-d}{e}\right)} + \frac{1-c}{1 + \exp\left(\frac{x-f}{g}\right)} \right] \quad (\text{S10})$$

$$y = a + bx + cx^2 + dx^3 + ex^4 + fx^5 + gx^6 \quad (\text{S11})$$

where  $a, b, c, d, e, f, g$  are fitting parameters.

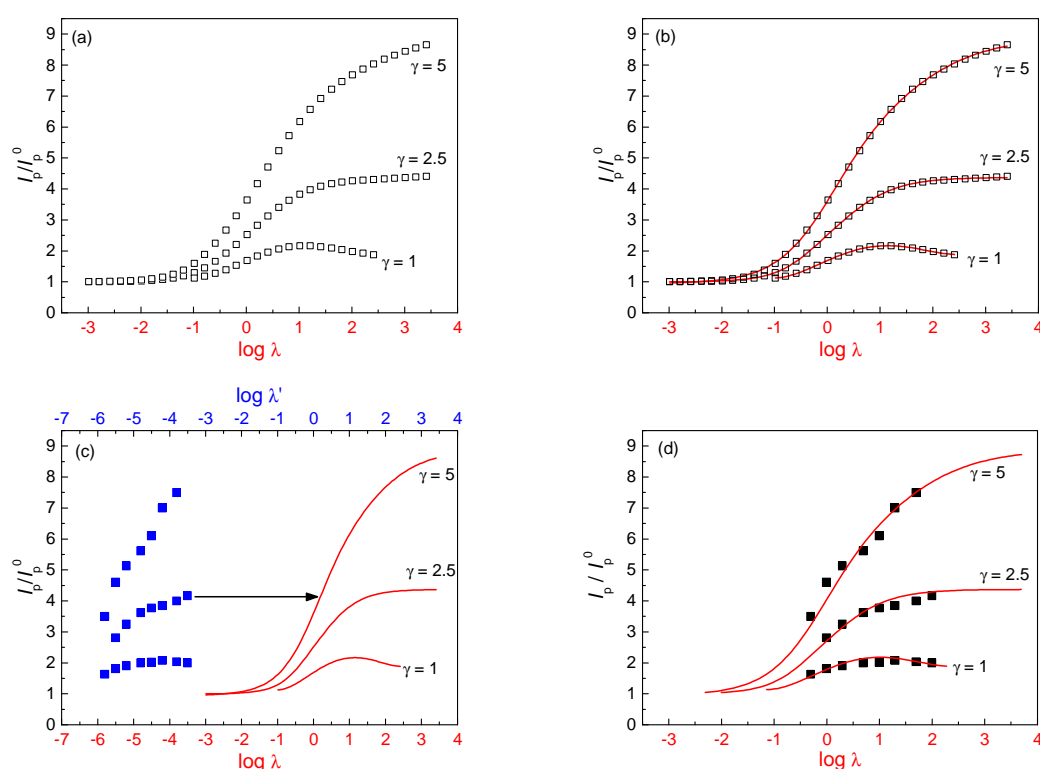


**Figure S5.** (a) Theoretical  $I_p/I_p^0$  versus  $\log \lambda = \log(RTk_{\text{act}}C_{[Cu^{II}L]^{2+}} / Fv)$  obtained from digital simulation of the CVs, considering the mechanism in eqs 2-8 (with  $[Cu^{II}Me_6TREN]^{2+}$  as catalyst and OEOBP as initiator). (b) Fitting of the theoretical  $I_p/I_p^0$  vs.  $\lambda$  to eqs S10 (for  $\gamma = 2.5$  and 5) and S11 (for  $\gamma = 1$ ). (c) Comparison of the experimental  $I_p/I_p^0$  vs.  $\log \lambda'$  (blue squares) with the theoretical working curves before the fitting procedure ( $\log \lambda' = \log(RTC_{[Cu^{II}L]^{2+}} / Fv)$ ). (d) Comparison of the experimental  $I_p/I_p^0$  vs.  $\log \lambda$  (black squares) with the theoretical working curves after the fitting procedure.

The procedure for the determination of  $k_{\text{act}}$  was as follows. The CV experiment was done with fixed values of  $\gamma$ . Then a set of  $I_p/I_p^0$  versus  $\log \lambda'$  values ( $\lambda' = RTC_{[\text{Cu}^{\text{II}}\text{L}]^{2+}} / Fv$ ) was calculated for each  $\gamma$  value (experimental points in Figure S5c). The theoretical working curves were then constructed (Figure S5a) and fitted to eq S10 or S11 to define the constants in the equation (Figure S5b). The experimental data were finally fitted to the appropriate equation by defining  $y = I_p/I_p^0$  and  $x = \log \lambda' + \log k_{\text{act}}$ , with  $k_{\text{act}}$  as the only adjustable parameter (Figure S5c-d).

### S6. Comparison between Experimental and Simulated CVs in the Presence of $[\text{Cu}^{\text{II}}\text{TPMA}]^{2+}$ and OEOBP.

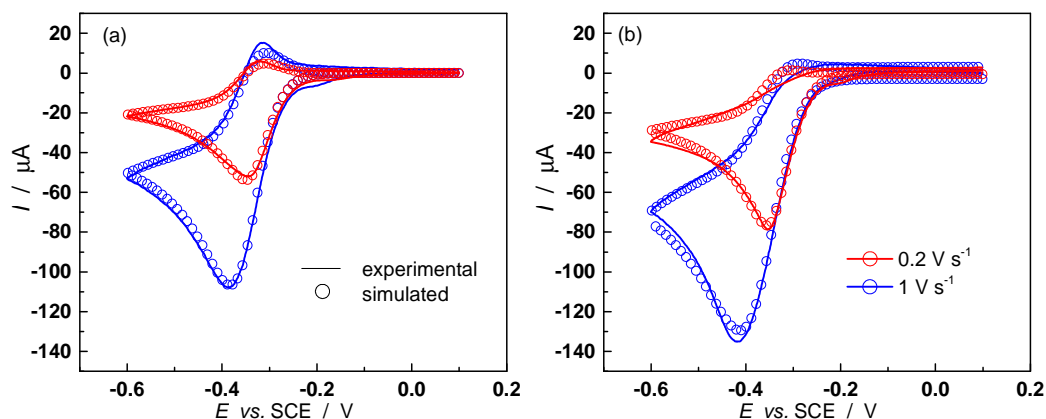


**Figure S6.** Comparison between experimental (solid lines) and simulated (circles) CVs of  $10^{-3} \text{ M}$   $[\text{Cu}^{\text{II}}\text{TPMA}]^{2+}$  in  $\text{H}_2\text{O} + 0.1 \text{ M Et}_4\text{NBF}_4$  at  $v = 0.2$  in the presence of (a)  $2 \times 10^{-3} \text{ M}$  or (b)  $3 \times 10^{-3} \text{ M}$  OEOBP.

## S7. Comparison of the CV Response in the Absence and in the Presence of Monomer

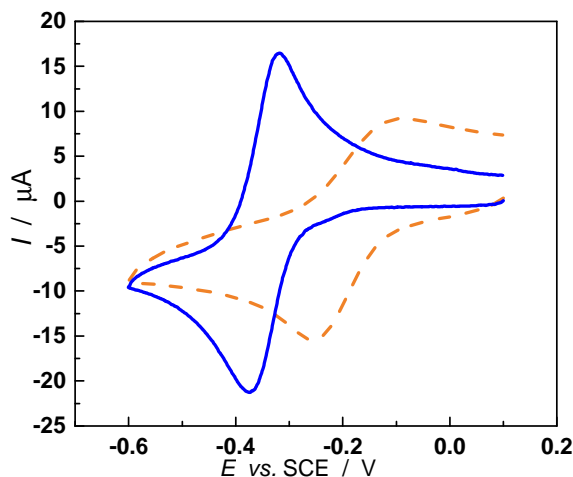


**Figure S7.** Cyclic voltammetry of  $10^{-3}$  M  $[\text{Cu}^{\text{II}}\text{TPMA}]^{2+}$  in water (solid line) and water-OEOA mixture (dashed line) recorded at  $0.2 \text{ V s}^{-1}$  in the presence of  $0.1 \text{ M Et}_4\text{NBF}_4$ .

## S7. Estimation of $K_{\text{ATRP}}$ for the $[\text{Cu}^{\text{I}}\text{L}]^+/\text{OEOBP}$ Systems

$K_{\text{ATRP}}$  was calculated as described in reference 8, from the following equation:<sup>8</sup>

$$\ln K_{\text{ATRP}} = \ln K_{\text{X}}^{\text{II}} + \frac{F}{RT} \left( E_{\text{X}^{\bullet}/\text{X}^-}^{\circ} - E_{[\text{Cu}^{\text{II}}\text{L}]^{2+}/[\text{Cu}^{\text{I}}\text{L}]^+}^{\circ} \right) - \frac{\Delta G_{\text{R-X}}}{RT} \quad (\text{S12})$$

where  $K_{\text{X}}^{\text{II}}$  is the halidophilicity constant,  $F$  is the Faraday constant,  $R$  is the gas constant, and  $\Delta G_{\text{R-X}}$  is bond dissociation free energy of the alkyl halide.

$K_{\text{X}}^{\text{II}}$  and  $E_{[\text{Cu}^{\text{II}}\text{L}]^{2+}/[\text{Cu}^{\text{I}}\text{L}]^+}^{\circ}$  values were obtained from reference 8, whereas the value for  $E_{\text{X}^{\bullet}/\text{X}^-}^{\circ}$  of the  $\text{Br}^{\bullet}/\text{Br}^-$  redox couple in water was obtained from reference 12. The bond dissociation free energy was calculated from the following equation:<sup>12</sup>

$$\Delta G_{\text{R-X(aq)}}^{\circ} = \text{BDE}_{(\text{g})} - T\Delta_{\text{BD}}S_{(\text{g})}^{\circ} + \Delta\Delta G_{\text{S}}^{\circ} \quad (\text{S13})$$

where  $BDE_{(g)}$  and  $\Delta_{BD}S_{(g)}^{\ominus}$  are the bond dissociation enthalpy and entropy in the gas phase, and  $\Delta\Delta G_S^{\ominus}$  is the difference in the solvation Gibbs free energy between products and reactants.  $BDE_{(g)}$  and  $\Delta_{BD}S_{(g)}^{\ominus}$  are not known for OEObP, therefore the values for methyl 2-bromopropionate were used,<sup>13</sup> considering that the pendant oligo(ethylene oxide) group has a small effect on the properties of the C-Br bond.  $\Delta\Delta G_S^{\ominus}$  is not known but was assumed to be negligible in agreement with previous reports.<sup>8</sup>

## References

- (1) Gahler, A. R. Colorimetric Determination of Copper with Neo-Cuproine. *Anal. Chem.* **1954**, *26*, 577-579.
- (2) Ye, J.; Xu, J.; Hu, J.; Wang, X.; Zhang, G.; Liu, S.; Wu, C. Comparative Study of Temperature-Induced Association of Cyclic and Linear Poly(N-Isopropylacrylamide) Chains in Dilute Solutions by Laser Light Scattering and Stopped-Flow Temperature Jump. *Macromolecules* **2008**, *41*, 4416-4422.
- (3) Konkolewicz, D.; Wang, Y.; Krys, P.; Zhong, M.; Isse, A. A.; Gennaro, A.; Matyjaszewski, K. SARA ATRP or SET-LRP. End of Controversy? *Polymer Chemistry* **2014**, *5*, 4396-4417.
- (4) Bard, A. J.; Faulkner, L. R. *Electrochemical Methods: Fundamentals and Applications*, 2nd Edition. Wiley & Sons: New York, NY, 2001.
- (5) Matyjaszewski, K.; Paik, H.-j.; Zhou, P.; Diamanti, S. J. Determination of Activation and Deactivation Rate Constants of Model Compounds in Atom Transfer Radical Polymerization. *Macromolecules* **2001**, *34*, 5125-5131.
- (6) Bowry, V. W.; Ingold, K. U. Kinetics of Nitroxide Radical Trapping. 2. Structural Effects. *J. Am. Chem. Soc.* **1992**, *114*, 4992-4996.

- (7) Skene, W. G.; Scaiano, J. C.; Listigovers, N. A.; Kazmaier, P. M.; Georges, M. K. Rate Constants for the Trapping of Various Carbon-Centered Radicals by Nitroxides: Unimolecular Initiators for Living Free Radical Polymerization. *Macromolecules* **2000**, *33*, 5065-5072.
- (8) Fantin, M.; Isse, A. A.; Gennaro, A.; Matyjaszewski, K. Understanding the Fundamentals of Aqueous ATRP and Defining Conditions for Better Control. *Macromolecules* **2015**, *48*, 6862-6875.
- (9) Konkolewicz, D.; Krys, P.; Góis, J. R.; Mendonça, P. V.; Zhong, M.; Wang, Y.; Gennaro, A.; Isse, A. A.; Fantin, M.; Matyjaszewski, K. Aqueous RDRP in the Presence of Cu(0): The Exceptional Activity of Cu(I) Confirms the SARA ATRP Mechanism. *Macromolecules* **2014**, *47*, 560-570.
- (10) Isse, A. A.; Berzi, G.; Falcicola, L.; Rossi, M.; Mussini, P. R.; Gennaro, A. Electrocatalysis and Electron Transfer Mechanisms in the Reduction of Organic Halides at Ag. *J. Appl. Electrochem.* **2009**, *39*, 2217.
- (11) Andrieux, C. P.; Blocman, C.; Dumas-Bouchiat, J. M.; M'Halla, F.; Savéant, J. M. Homogeneous Redox Catalysis of Electrochemical Reactions: Part V. Cyclic Voltammetry. *J. Electroanal. Chem. Interfacial Electrochem.* **1980**, *113*, 19-40.
- (12) Isse, A. A.; Lin, C. Y.; Coote, M. L.; Gennaro, A. Estimation of Standard Reduction Potentials of Halogen Atoms and Alkyl Halides. *J. Phys. Chem. B* **2011**, *115*, 678-684.
- (13) Lin, C. Y.; Coote, M. L.; Gennaro, A.; Matyjaszewski, K. Ab Initio Evaluation of the Thermodynamic and Electrochemical Properties of Alkyl Halides and Radicals and Their Mechanistic Implications for Atom Transfer Radical Polymerization. *J. Am. Chem. Soc.* **2008**, *130*, 12762-12774.